CEAS EuroGNC 2019
"Conference on Guidance, Navigation and Control"
3-5 April 2019 @ Politecnico di Milano, Milan, Italy.

CEAS-GNC-2019-045

Study of Impact Point Prediction Methods for Zero-Effort-Miss Guidance: Application to a 155 mm Spin-Stabilized Guided Projectile

Michael Proff and Spilios Theodoulis

Abstract The increased precision demands of artillery shells require adapted guidance techniques improving the overall impact probability. To this end, the impact point must be estimated by an Impact Point Prediction (IPP) method in order to correct the ballistic trajectory to hit the target. This paper presents a novel IPP method for the Zero-Effort-Miss (ZEM) guidance techniques based on a Modified Point Mass (MPM) model. The development is focused on improving the IPP accuracy by identifying the roots of uncertainty of existing methods. Nominal trajectory simulation results show a large improvement in the IPP fidelity leading to lower guidance accelerations and actuator demands. This results are confirmed by Monte-Carlo trajectory simulations with uncertainties in launch condition, aerodynamics and environment.

1 Introduction

Higher operational requirements in range in order to combat distant targets, and accuracy in order to reduce collateral damage and necessary number of rounds per target, create the need for guided ammunition. The control mechanisms to steer these systems range from aerodynamic surfaces [4, 9, 10, 11] over jet thrusters [1, 2, 7] to inertial loads [10]. The stability of the projectile is guaranteed either dynamic by fins located at the tail or gyroscopic by a high axial spin rate.

The increased precision demands of artillery shells require new guidance techniques improving the overall impact probability. To this end, the impact point must be estimated by an Impact Point Prediction (IPP) method in order to correct the

Michael Proff
Guidance, Navigation & Control Dept., ISL - French-German Research Institute of Saint-Louis, 68300 Saint-Louis, France, e-mail: Michael.Proff@isl.eu

Spilios Theodoulis
Guidance, Navigation & Control Dept., ISL - French-German Research Institute of Saint-Louis, 68300 Saint-Louis, France, e-mail: Spilios.Theodoulis@isl.eu

ballistic trajectory to hit the target. This paper presents a developed IPP method for the Zero-Effort-Miss (ZEM) guidance techniques based on a modified point mass model. The development is focused on improving the IPP accuracy by identifying the origins of uncertainty of existing methods. Nominal trajectory simulation results show a large improvement in the IPP fidelity leading to lower guidance accelerations and actuator demands. This results are confirmed in the Monte-Carlo trajectory simulations with uncertainties in launch condition, aerodynamics and environment though with perfect navigation.

The control of the projectile used in this work is performed by four canards located at the nose, thus offering a continues time trajectory correction. Low unit costs favor the usage of existing spin-stabilized projectiles shells retrofitted with roll-decoupled Course Correction Fuzes (CCF). This concept has a strong coupling between pitch/yaw dynamics and has a limited amount of control authority due to its high spin.

The maneuverability characteristics of the projectile demand a well functioning interaction between guidance and control in order to enable the maximum miss distance correction for a given angular amplitude of the canard actuator. Therefore, it is necessary for the guidance to consider the natural ballistic behavior of a spin-stabilized projectile.

Proportional Navigation (PN) and Zero-Effort-Miss (ZEM) guidance based techniques [14] are evaluated with a reduced-order $\mathcal{H}_\infty$ control designed autopilot [12]. Traditionally, PN guidance minimizes the Line-of-Sight (LoS) rate between interceptor and target resulting in an ideal collision course of a direct straight line, not matching the ballistic trajectory and requiring relatively large actuator deflections. ZEM guidance techniques though, correct the miss distance by commanding a compensating acceleration which is proportional to the magnitude of the offset and divided by the square of the remaining flight time. The offset is determined by the difference between the location estimated by the Impact Point Prediction (IPP) algorithm and the target. The existing Modified Point Mass (MPM) [8, 6] IPP model uses several simplifications leading to lower accuracy and higher actuator deflections. These are examined and resolved in a second MPM model and evaluated against PN and the first ZEM MPM IPP for nominal and Monte-Carlo trajectories.

The paper is structured as follows: Section 2 outlines the projectile concept and its non-linear airframe model and properties, Section 3 presents the Zero-Effort-Miss (ZEM) guidance technique, gives and overview of existing Impact Point Prediction (IPP) methods and describes the further development of a Modified Point Mass (MPM) to achieve higher accuracy, and finally Section 4 shows the performance improvement of the developed MPM IPP in nominal and Monte-Carlo trajectory simulations.

2 Projectile Concept

The concept of the airframe (Fig. 1) is a dual-spin projectile with a roll-decoupled Course Correction Fuze (CCF) . The aft part of the airframe holding the payload spins with a frequency comparable to existing unguided spin-stabilized projectiles. The roll-decoupled CCF is fitted with four independent actuators. Each one drives a canard for continuous aerodynamic trajectory correction using the Skid-To-Turn (STT) nose configuration. All necessary hardware such as sensors, actuators and processors (guidance & control) are located in the fuze [12].

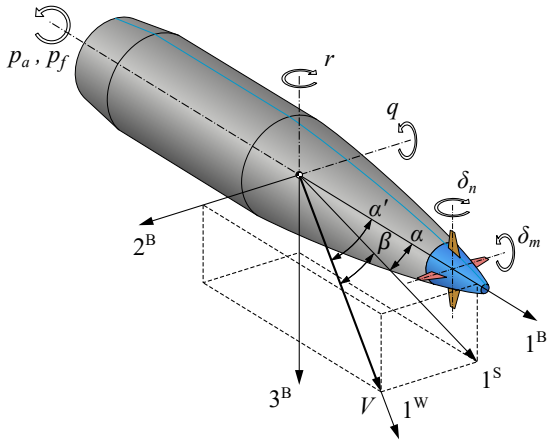

Fig. 1 ISL 155 mm course correction fuze concept [12]

2.1 Nonlinear Dynamics and Kinematics

The nonlinear 7DoF model for ballistic dual-spin projectiles [3] was extended for guidance in [13, 11, 12] and is given below. The projectile translational and attitude dynamics, written in the body non-rolling frame (BNR, denoted by B′) and projected in the related body Coordinate System (CS), are:

$$\begin{bmatrix}\dot{u}\\ \dot{v}\\ \dot{w}\end{bmatrix}^{\mathrm{B}'} = \frac{1}{m}\begin{bmatrix}X\\ Y\\ Z\end{bmatrix}^{\mathrm{B}'} - \begin{bmatrix}0 & -r & q\\ r & 0 & r\tan\Theta\\ -q & -r\tan\Theta & 0\end{bmatrix}\begin{bmatrix}u\\ v\\ w\end{bmatrix}^{\mathrm{B}'} \tag{1}$$

$$\begin{bmatrix}\dot{p}_\mathrm{f}\\ \dot{p}_\mathrm{a}\\ \dot{q}\\ \dot{r}\end{bmatrix}^{\mathrm{B}'} = \boldsymbol{I}^{-1}\left(\begin{bmatrix}L_\mathrm{f}\\ L_\mathrm{a}\\ M\\ N\end{bmatrix}^{\mathrm{B}'} - \left[\begin{array}{c|ccc}0 & 0 & -r & q\\ \hline 0 & 0 & -r & q\\ 0 & r & 0 & r\tan\Theta\\ 0 & -q & -r\tan\Theta & 0\end{array}\right]\boldsymbol{I}\begin{bmatrix}p_\mathrm{f}\\ p_\mathrm{a}\\ q\\ r\end{bmatrix}^{\mathrm{B}'}\right) \tag{2}$$

The projectile translational and attitude kinematics, written in the BNR and projected on the local-level L or North east down (NED) CS, are:

$$\begin{bmatrix}\dot{x}\\ \dot{y}\\ \dot{z}\end{bmatrix}^{\mathrm{L}} = \begin{bmatrix}\cos\Theta\cos\Psi & -\sin\Psi & \sin\Theta\cos\Psi\\ \cos\Theta\sin\Psi & \cos\Psi & \sin\Theta\sin\Psi\\ \sin\Theta & 0 & \cos\Theta\end{bmatrix}\begin{bmatrix}u\\ v\\ w\end{bmatrix}^{\mathrm{B}'} \tag{3}$$

$$\left[\begin{array}{c}\dot{\Phi}_{\mathrm{f}}\\ \hline \dot{\Phi}_{\mathrm{a}}\\ \dot{\Theta}\\ \dot{\Psi}\end{array}\right] = \left[\begin{array}{c|ccc}1 & 0 & 0 & \tan\Theta\\ \hline 0 & 1 & 0 & \tan\Theta\\ 0 & 0 & 1 & 0\\ 0 & 0 & 0 & \sec\Theta\end{array}\right]\left[\begin{array}{c}p_{\mathrm{f}}\\ \hline p_{\mathrm{a}}\\ q\\ r\end{array}\right]^{\mathrm{B}'} \tag{4}$$

The dynamic states of the system are the linear (u, v, w) and angular $(p_{\mathrm{f}}, p_{\mathrm{a}}, q, r)$ velocities, and the kinematic states are the linear $(x_{\mathrm{L}}, y_{\mathrm{L}}, z_{\mathrm{L}})$ and angular $(\Phi_{\mathrm{f}}, \Phi_{\mathrm{a}}, \Theta, \Psi)$ positions.[1]

The external forces acting on the airframe (X, Y, Z) result from the following aerodynamic (body B, canard C and Magnus M) and gravity (G) components:

$$\begin{aligned}\begin{bmatrix}X\\ Y\\ Z\end{bmatrix} &= \begin{bmatrix}X_{\mathrm{B}}\\ Y_{\mathrm{B}}\\ Y_{\mathrm{B}}\end{bmatrix} + \begin{bmatrix}X_{\mathrm{C}}\\ Y_{\mathrm{C}}\\ Y_{\mathrm{C}}\end{bmatrix} + \begin{bmatrix}X_{\mathrm{M}}\\ Y_{\mathrm{M}}\\ Y_{\mathrm{M}}\end{bmatrix} + \begin{bmatrix}X_{\mathrm{G}}\\ Y_{\mathrm{G}}\\ Y_{\mathrm{G}}\end{bmatrix}\\ &= \bar{q}S\left(\begin{bmatrix}-C_{\mathrm{A}}\\ C_{\mathrm{Y}\beta}\beta\\ C_{\mathrm{N}\alpha}\alpha\end{bmatrix} + \begin{bmatrix}0\\ C_{\mathrm{Y}\delta}\delta_{\mathrm{n}}\\ C_{\mathrm{N}\delta}\delta_{\mathrm{m}}\end{bmatrix}\begin{bmatrix}0\\ -C_{\mathrm{Y}p\alpha}\alpha\\ C_{\mathrm{Y}p\alpha}\beta\end{bmatrix}\right) + mg\begin{bmatrix}-\sin\Theta\\ 0\\ \cos\Theta\end{bmatrix}\end{aligned} \tag{5}$$

The external moments acting on the airframe $(L_{\mathrm{f}}, L_{\mathrm{a}}, M, N)$ contain additional aerodynamic damping D and mechanical friction F components, whereas gravity has no component:

$$\begin{aligned}\left[\begin{array}{c}L_{\mathrm{f}}\\ \hline L_{\mathrm{a}}\\ M\\ N\end{array}\right] &= \left[\begin{array}{c}L_{\mathrm{Bf}}\\ \hline L_{\mathrm{Ba}}\\ M_{\mathrm{B}}\\ N_{\mathrm{B}}\end{array}\right] + \left[\begin{array}{c}L_{\mathrm{Cf}}\\ \hline L_{\mathrm{Ca}}\\ M_{\mathrm{C}}\\ N_{\mathrm{C}}\end{array}\right] + \left[\begin{array}{c}L_{\mathrm{Mf}}\\ \hline L_{\mathrm{Ma}}\\ M_{\mathrm{M}}\\ N_{\mathrm{M}}\end{array}\right] + \left[\begin{array}{c}L_{\mathrm{Df}}\\ \hline L_{\mathrm{Da}}\\ M_{\mathrm{D}}\\ N_{\mathrm{D}}\end{array}\right] + \left[\begin{array}{c}L_{\mathrm{Ff}}\\ \hline L_{\mathrm{Fa}}\\ M_{\mathrm{F}}\\ N_{\mathrm{F}}\end{array}\right]\\ &= \bar{q}S\left(\left[\begin{array}{c}0\\ \hline 0\\ C_{\mathrm{m}\alpha}\alpha\\ C_{\mathrm{n}\beta}\beta\end{array}\right] + \frac{p_{\mathrm{a}}d}{V}\left[\begin{array}{c}C_{\mathrm{l}\delta}\delta_{\mathrm{p}}\\ \hline 0\\ C_{\mathrm{m}\delta}\delta_{\mathrm{q}}\\ C_{\mathrm{n}\delta}\delta_{\mathrm{r}}\end{array}\right] + \frac{d}{V}\left[\begin{array}{c}0\\ \hline C_{\mathrm{l}p}p_{\mathrm{a}}\\ C_{\mathrm{m}q}q\\ C_{\mathrm{n}r}r\end{array}\right]\right) + \left[\begin{array}{c}L_{\mathrm{f-a}}\\ \hline -L_{\mathrm{f-a}}\\ 0\\ 0\end{array}\right]\end{aligned} \tag{6}$$

The friction moment $L_{\mathrm{f-a}}$ between the forward and aft parts is modeled using the viscous friction coefficient K_{v} by

$$L_{\mathrm{f-a}} = K_{\mathrm{v}}\,(p_{\mathrm{a}} - p_{\mathrm{f}}) \tag{7}$$

[1] Subscripts 'f' and 'a' represent respectably 'forward' and 'aft' part-related constants or variables

The control variables $\delta_p, \delta_q, \delta_r$ are virtual signals depending on the angular position of the fuze Φ_f, the allocation matrix $[\boldsymbol{T}]^{\mathrm{VR}}$ and the real canard deflection angles $\delta_1, \delta_2, \delta_3, \delta_4$ satisfying:

$$\begin{bmatrix}\delta_p\\ \delta_q\\ \delta_r\end{bmatrix}^{\mathrm{B}'_\mathrm{a}} = [\boldsymbol{T}(\Phi_\mathrm{f})]^{\mathrm{B}'_\mathrm{a}\mathrm{B}_\mathrm{f}}\,[\boldsymbol{T}]^{\mathrm{VR}}\begin{bmatrix}\delta_1\\ \delta_2\\ \delta_3\\ \delta_4\end{bmatrix}^{\mathrm{B}_\mathrm{f}} = \begin{bmatrix}1 & 0 & 0\\ 0 & \cos\Phi_\mathrm{f} & -\sin\Phi_\mathrm{f}\\ 0 & \sin\Phi_\mathrm{f} & \cos\Phi_\mathrm{f}\end{bmatrix}\begin{bmatrix}¼ & ¼ & -¼ & -¼\\ 0 & ½ & 0 & ½\\ ½ & 0 & ½ & 0\end{bmatrix}\begin{bmatrix}\delta_1\\ \delta_2\\ \delta_3\\ \delta_4\end{bmatrix} \quad (8)$$

The terms $C_\mathrm{A}, C_{\mathrm{Y}\beta}, C_{\mathrm{N}\alpha}$ (with $C_{\mathrm{Y}\beta} = -C_{\mathrm{N}\alpha}$)[2] are the body, $C_{\mathrm{N}\delta}, C_{\mathrm{Y}\delta}$ (with $C_{\mathrm{Y}\delta} = C_{\mathrm{N}\delta}$) the canard and $C_{\mathrm{Y}p\alpha}$ the Magnus force aerodynamic coefficients. The terms $C_{\mathrm{m}\alpha}, C_{\mathrm{n}\beta}$ (with $C_{\mathrm{n}\beta} = -C_{\mathrm{m}\alpha}$) are the body, $C_{\mathrm{m}\delta}, C_{\mathrm{n}\delta}$ (with $C_{\mathrm{n}\delta} = C_{\mathrm{m}\delta}$) the canard, $C_{\mathrm{l}p}, C_{\mathrm{m}q}, C_{\mathrm{n}r}$ (with $C_{\mathrm{n}r} = C_{\mathrm{m}q}$) the damping and $C_{\mathrm{n}p\alpha}$ the Magnus moment aerodynamic coefficients. These are a non-linear function of the Mach number $\mathcal{M}$ and the Angle of Incidence (AoI) α'. The velocity of the airframe V, the Angle of Attack (AoA) α, the Angle of Sideslip (AoS) β and AoI are visualized in Fig. 1 and defined as [15]:

$$V = \sqrt{u^2 + v^2 + w^2} \quad (9)$$

$$\alpha = \arctan\left(\frac{w}{u}\right) \quad (10)$$

$$\beta = \arcsin\left(\frac{v}{V}\right) = \arctan\left(\frac{v}{\sqrt{u^2 + w^2}}\right) \quad (11)$$

$$\alpha' = \arccos\left(\frac{u}{V}\right) = \arccos\left(\cos\alpha\cos\beta\right) \quad (12)$$

2.2 Autopilot

The autopilot is designed as a Skid-To-Turn (STT) nose controlled configuration using $\mathcal{H}_\infty$ control techniques to achieve the performance, robustness and stability requirements with at the same time least complexity. Therefore, the autopilot is divided into a roll and a pitch/yaw channel [12].

The roll channel controls the angular position Φ_f of the decoupled fuze, which is set to zero for the STT resulting in a "+" configuration (Fig.1). The initial roll rate of the fuze due to the bearing friction has to be reduced to zero to achieve this configuration from the initial state at the beginning of the controlled phase. The input signals of the roll controller are the commanded roll position $\Phi_{\mathrm{f,cmd}}$, and the measured roll position $\tilde{\Phi}_\mathrm{f}$ and roll rate $\tilde{p}_\mathrm{f}$ of the fuze. The output signal is the virtual

[2] This assumption is valid due to the rotational symmetry of the projectile body giving a direct relation between the forces and moments coefficients of the longitudinal and lateral plane

roll deflection angle δ_p of the canards. The internal structure of the roll channel consists of a proportional controller for the angular rate and a P/PI regulator/servo controller for the angular position.

The highly coupled pitch/yaw channel controls the specific accelerations of the projectile in the vertical $x_{B'}$ and lateral $y_{B'}$ direction (Fig.1), by using two orthogonal pairs of opposite canards for the pitch and yaw channel of the "+" configuration. The input signals of the pitch/yaw controller are the measured normal $\tilde{n}_\mathrm{z}$ and lateral $\tilde{n}_\mathrm{y}$ accelerations, the measured pitch $\tilde{q}$ and yaw $\tilde{r}$ rates, and the commanded normal $n_\mathrm{z,cmd}$ and lateral $n_\mathrm{y,cmd}$ accelerations. The controller outputs are the pitch δ_q and yaw δ_r virtual canard deflection angles. The internal structure of the pitch/yaw channel consists of a feedforward controller for the commanded accelerations, a servo controller for the difference between commanded and measured accelerations and a regulation controller for the measured accelerations and angular rates (pitch/yaw) [12].

3 Zero-Effort-Miss

The Zero-Effort-Miss (ZEM) is a guidance technique using the difference between the estimated no-action impact point (considering the current state of the projectile as initial condition) and the mission target position to provide a guidance command. The position offset is given by [14, 6]:

$$\mathrm{ZEM_x} = x(t_\mathrm{go}) - x_\mathrm{t} \tag{13a}$$

$$\mathrm{ZEM_y} = y(t_\mathrm{go}) - y_\mathrm{t} \tag{13b}$$

where $\mathrm{ZEM_x}$ and $\mathrm{ZEM_y}$ are the longitudinal and lateral offsets, and $x(t_\mathrm{go})$ and $y(t_\mathrm{go})$ the estimated impact longitudinal and lateral position (as a function of the time to go t_go) by using an Impact Point Prediction (IPP) method (Sec. 3.1). The mission target is defined by the longitudinal x_t and lateral y_t coordinates.

The proposed leads to the general guidance acceleration command by the position offset from Eq.13 as [6]:

$$\boldsymbol{a}_\mathrm{go} = k_\mathrm{g} \begin{bmatrix} -\mathrm{ZEM_x} & -\mathrm{ZEM_y} & 0 \end{bmatrix}^\mathsf{T} \tag{14}$$

Due to the fact, that a guided projectile is not able to produce thrust in most cases, the acceleration in the longitudinal direction of the projectile is converted to a normal acceleration. This is done by inverting the sign of the longitudinal offset and writing it as normal component. In the case of a positive flight path angle γ in combination with an initial launch angle Θ_0 greater than $45° = \frac{\pi}{4}$, the direction of the normal acceleration is already acting in the correct sense and needs no sign inversion. This leads to the following expression [6]:

$$\boldsymbol{a}_\mathrm{go} = \begin{cases} k_\mathrm{g} \begin{bmatrix} 0 & -\mathrm{ZEM_y} & -\mathrm{ZEM_x} \end{bmatrix}^\mathsf{T}, & \text{if } \Theta_0 > \frac{\pi}{4} \text{ and } \gamma > 0 \\ k_\mathrm{g} \begin{bmatrix} 0 & -\mathrm{ZEM_y} & +\mathrm{ZEM_x} \end{bmatrix}^\mathsf{T}, & \text{otherwise} \end{cases} \tag{15}$$

The ZEM guidance gain k_g is defined by the quotient of the navigation gain N divided by the time to go squared [6].

$$k_g = \frac{N}{\left(t_{go}\right)^2} \tag{16}$$

Hence, the ZEM guidance gain is ∞ for the impact time ($t_{go} \rightarrow 0$), it cannot be used for the endgame. Either the guidance gain has to be bounded (e.g. considering a maximum k_g leading to a tolerated minimum time to go t_{go}) or another guidance technique (e.g. Proportional Navigation (PN)) has to be considered for this terminal phase.

The sum of the guidance acceleration command $\boldsymbol{a}_{go}$ and the current specific acceleration $\boldsymbol{a}_{eo}$ (Sec. 3.2) acting on the projectile are divided by the gravity constant g in order to receive a normalized acceleration command $\boldsymbol{a}_{cmd}$ for the autopilot:

$$\boldsymbol{a}_{cmd} = \frac{\boldsymbol{a}_{go} + \boldsymbol{a}_{eo}}{g} \tag{17}$$

3.1 Impact Point Prediction Methods

The existing impact point prediction (IPP) methods can be attributed to one ore more of the following seven categories which are ordered with decreasing complexity in the perspective of the model and the necessary initial states and parameters [5]:

- Six-Degrees-of-Freedom rigid body (6DoF)
- Modified-Linear Theory (MLT)
- Modified Point Mass (MPM)
- Full Point Mass (FPM)
- Simple Point Mass (SPM)
- Hybrid Point Mass (HPM)
- Vacuum Point Mass (VPM)

An overview of the initial states and obligatory parameters are given for each IPP method (Tab. 1).

The most complex IPP is a full Six-Degrees-of-Freedom rigid body (6DoF) model which demands 12 initial states to describe all translational and angular positions and velocities. Additional obligatory parameters are the environmental data as gravity constant g, density ρ and speed of sound a, the properties of the projectile such as caliber d, mass m, inertia tensor $\boldsymbol{I}$ and location of the center of gravity CG, and finally the complete set of aerodynamic coefficients.

A closed-form solution and therefore simplification of the 6DoF model is the Modified-Linear Theory (MLT) model. The same initial states as for the 6DoF model are required but the model is in terms of parameters and equations to solve less complex. It neglects the higher order aerodynamic coefficient terms and the

Table 1 Summary of IPP required states and parameters [5]

IPP	States	Parameters
6DoF	x, y, z, Φ, Θ, Ψ, $\tilde{u}$, $\tilde{v}$, $\tilde{w}$, $\tilde{p}$, $\tilde{q}$, $\tilde{r}$	g, ρ, a, m, d, $\boldsymbol{I}$, CG, C_{X0}, $C_{\mathrm{X}\alpha 2}$, $C_{\mathrm{N}\alpha}$, $C_{\mathrm{Y}p\alpha}$, $C_{\mathrm{m}\alpha}$, $C_{\mathrm{m}q}$, $C_{\mathrm{n}p\alpha}$, $C_{\mathrm{l}p}$
MLT	x', y', z', Φ', Θ', Ψ', $\tilde{u}'$, $\tilde{v}'$, $\tilde{w}'$, $\tilde{p}'$, $\tilde{q}'$, $\tilde{r}'$	g, ρ, a, m, d, I_{xx}, I_{yy}, CG, C_{X0}, $C_{\mathrm{N}\alpha}$, $C_{\mathrm{m}\alpha}$, $C_{\mathrm{m}q}$, $C_{\mathrm{n}p\alpha}$, $C_{\mathrm{l}p}$
MPM	x, y, z, $\dot{x}$, $\dot{y}$, $\dot{z}$, $\dot{\Phi}$	g, ρ, a, m, d, I_{xx}, CG, C_{X0}, $C_{\mathrm{X}\alpha 2}$, $C_{\mathrm{N}\alpha}$, $C_{\mathrm{Y}p\alpha}$, $C_{\mathrm{m}\alpha}$, $C_{\mathrm{l}p}$
FPM	x, y, z, $\dot{x}$, $\dot{y}$, $\dot{z}$	g, ρ, a, m, d, C_{X0}
SPM	x, y, z, $\dot{x}$, $\dot{y}$, $\dot{z}$	g, ρ, a, m, d, C_{X0}
HPM	x, y, z, $\dot{x}$, $\dot{y}$, $\dot{z}$	g, ρ, a, m, d, C_{X0}
VPM	x, y, z, $\dot{x}$, $\dot{y}$, $\dot{z}$	g

Magnus force coefficient, and at the same time simplifies the inertia tensor for symmetric projectiles by reducing it to an axial and a transverse component.

The Modified Point Mass (MPM) model represents the projectile as a point mass with an additional term for the spin rate. Hereby, the spin rate is compulsory to consider the drift in the crossrange direction due to the yaw of repose (Sec. 3.2). The initial states of the MPM model are the translational positions and velocities as well as the initial spin rate. The required parameters are the same as for the MLT model except for the additional non-linearity term of the axial force coefficient $C_{\mathrm{X}\alpha 2}$. Additionally the transverse moment of inertia I_{yy} is neglected.

The Full Point Mass (FPM), Simple Point Mass (SPM), Hybrid Point Mass (HPM) and Vacuum Point Mass (VPM) models express the motion of the projectile as a point mass. These models all have the translational positions and velocities as initial states. FPM, SPM and HPM require as parameters the gravity constant g, density ρ and speed of sound a, the properties of the projectile such as caliber d, mass m and the zero incidence axial force coefficient C_{X0}. For the reason that the VPM describes the atmosphere as a vacuum only gravity is acting on the projectile which reduces the parameters to the gravity constant g for that model. The differences between FPM, SPM and HPM lie in the modeling of the forces acting on the projectile. For the FPM the density ρ and zero incidence axial force coefficient C_{X0} are updated during flight. The SPM uses instead the parameters at gun launch for the entire trajectory computation. The HPM is based on vacuum-type equations of motion but additionally includes an updated drag estimate [5].

3.2 Modified Point Mass Model with Dual Regime Algorithm

The Modified Point Mass (MPM) model with dual regime algorithm [8, 6] simulates the translational motion of the projectile considering the gravity, drag, lift and Magnus forces which are acting on it. It is called dual regime algorithm because it uses different coefficients for supersonic and subsonic flight and treats them as separated steps. The closed-form solution is evaluated twice (for supersonic and

subsonic regime separately) if the projectile is initially supersonic and only once if subsonic, assuming that it is not turning supersonic again for the remaining trajectory. For the supersonic case, the results of the closed-form solution are used as initial states for the subsonic regime.

The MPM model uses drag, lift, Magnus and gravity force to retrieve the accelerations affecting the projectile trajectory. The drag force acts in the opposite direction of the projectile velocity

$$\boldsymbol{f}_{\mathrm{D}} = -\bar{q}SC_{\mathrm{D}}\frac{\boldsymbol{v}}{\|\boldsymbol{v}\|} \tag{18}$$

The yaw of repose vector $\boldsymbol{\alpha}_{\mathrm{r}}$ is used for determining the total incidence of the projectile and is perpendicular to the plane formed by the gravity and velocity vectors.

$$\boldsymbol{\alpha}_{\mathrm{r}} = \frac{I_{\mathrm{xx}}p}{\bar{q}SdC_{\mathrm{m}\alpha}}\left(\boldsymbol{g}\times\frac{\boldsymbol{v}}{\|\boldsymbol{v}\|}\right) \tag{19}$$

The lift force is then parallel to the yaw of repose and therefore

$$\boldsymbol{f}_{\mathrm{L}} = \bar{q}SC_{\mathrm{L}\alpha}\boldsymbol{\alpha}_{\mathrm{r}} \tag{20}$$

The Magnus force is perpendicular to the plane formed by the velocity and yaw of repose vectors

$$\boldsymbol{f}_{\mathrm{M}} = \bar{q}SC_{\mathrm{Y}p\alpha}\frac{pd}{2\|\boldsymbol{v}\|}\left(\frac{\boldsymbol{v}}{\|\boldsymbol{v}\|}\times\boldsymbol{\alpha}_{\mathrm{r}}\right) \tag{21}$$

Using Eqs. 18 to 21 the point mass equation is written as [6]:

$$m\dot{\boldsymbol{v}} = \boldsymbol{f}_{\mathrm{D}} + m\boldsymbol{g} + \boldsymbol{f}_{\mathrm{L}} + \boldsymbol{f}_{\mathrm{M}} \tag{22}$$

The point mass Eq. 22 is arranged in a Line-of-Sight (LoS) CS to the target which has its origin in the cannon, with its x-axis and y-axis in the horizontal plane, requiring no additional transformations. The x-axis of the CS is parallel to the cannon muzzle azimuth and in downrange direction, the z-axis down and the y-axis to the right [6].

In order to reduce the workload of the autopilot, the specific acceleration by the aerodynamic forces of the projectile are needed and approximated by the following equation

$$\boldsymbol{a}_{\mathbf{eo}} = \frac{\bar{q}S\left(-C_{\mathrm{D}}\frac{\boldsymbol{v}}{\|\boldsymbol{v}\|} + C_{\mathrm{L}\alpha}\boldsymbol{\alpha}_{\mathrm{r}} + C_{\mathrm{Y}p\alpha}\frac{pd}{2\|\boldsymbol{v}\|}\left(\frac{\boldsymbol{v}}{\|\boldsymbol{v}\|}\times\boldsymbol{\alpha}_{\mathrm{r}}\right)\right)}{m} \tag{23}$$

3.3 Modified Point Mass Model with Variable Spin Rate and Parameters

Trajectory simulations using the MPM dual regime algorithm (Sec. 3.2) did not provide an acceptable accuracy for the impact location (Sec. 4.1) because of a predicted offset of more than 40 m downrange and 20 m crossrange for the nominal trajectory and a guidance start at $t = 60$ s. Therefore the roots of inaccuracy of the algorithm are identified and improvements developed.

The MPM dual regime algorithm uses the following assumptions:

- Constant coefficients $C_{\mathrm{D}}, C_{\mathrm{L}\alpha}, C_{\mathrm{Y}p\alpha}$ and $C_{\mathrm{m}\alpha}$
- Constant spin rate p for the Magnus force
- Constant angle of repose α_{r}
- Simplifications for the integration method and equations

3.3.1 Constant Coefficients

The assumption that the coefficients of the projectile are constant (for each regime) throughout the flight is problematic when looking at the variation of the coefficients between the guidance start $t = 60$ s and impact (Fig. 2). This gets even more critical if the projectile turns supersonic again after being subsonic or if it is operated over a wide range of possible Mach numbers $\mathcal{M}$. The solution proposed is to update the aerodynamic coefficients for each flight point of the remaining trajectory with respect to the Mach number $\mathcal{M}$ and Angle of Attack (AoA) α and Angle of Sideslip (AoS) β using the nominal projectile aerodynamic coefficients.

3.3.2 Constant Spin Rate

The Magnus force is linear to the Magnus force coefficient $C_{\mathrm{Y}p\alpha}$ and the spin rate p. The MPM Dual Regime algorithm considers the spin rate to be constant during the remaining flight time, which is not the case because of the roll damping moment of the body. Therefore, the variation in spin rate has to be taken into account for the computation of the Magnus force, especially when the remaining flight time for the IPP is increased. Below the spin rate of the nominal ballistic trajectory is shown between guidance start $t = 60$ s and impact (Fig. 3).

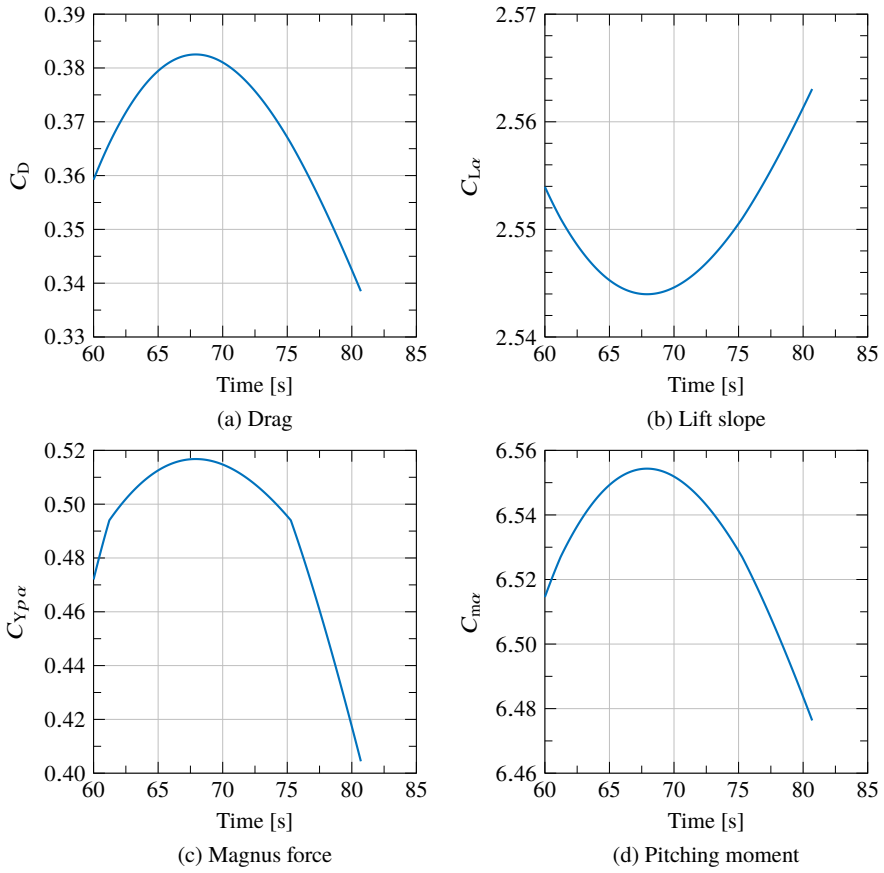

Fig. 2 Aerodynamic coefficients along a nominal ballistic trajectory (Sec. 4.1)

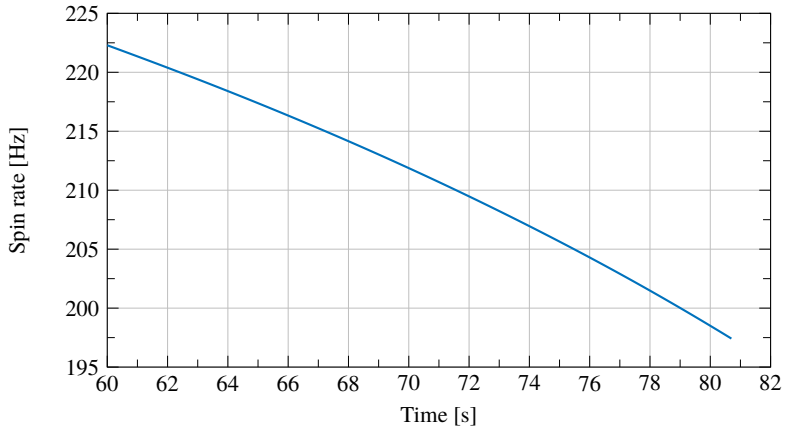

Fig. 3 Spin rate of nominal ballistic trajectory (Sec. 4.1)

3.3.3 Constant Yaw of Repose

The yaw of repose vector $\boldsymbol{\alpha}_\mathrm{r}$ is in the MPM Dual Regime algorithm only considered as a constant vector. For the α-plane this simplifications seem to be valid for the nominal ballistic trajectory and a guidance start at $t = 60\,\mathrm{s}$ but the β-plane varies a lot in the same time and cannot therefore be considered as constant (Fig. 4). The same problem arises for the α-plane of a non-nominal trajectory where the projectile achieves higher incidences than in the nominal one. To improve the accuracy of the impact prediction, all those variations have to be accounted for by updating the yaw of repose vector $\boldsymbol{\alpha}_\mathrm{r}$ during each flight point of the remaining trajectory using Eq. 19.

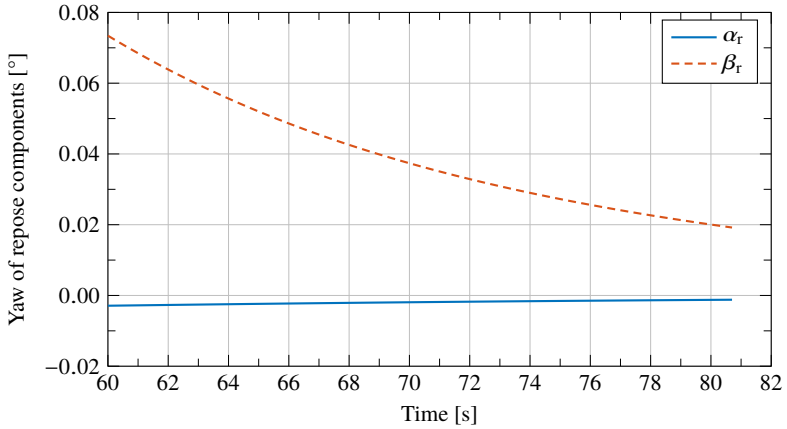

Fig. 4 Yaw of repose components of nominal ballistic trajectory (Sec. 4.1)

3.3.4 Simplifications for the Integration Method and Equations

The MPM Dual Regime impact location prediction algorithm uses one single time interval for the integration, by supposing a constant acceleration during this interval. Furthermore, the x- and z-axis dynamics are modeled by time-invariant linear differential equations. The solution proposed in this work to the problem of having constant signals (such as the accelerations in this case) during the integration period, is to split the integration into multiple (and thus smaller) time intervals. In this way the aforementioned signals are obtained in a more accurate and smooth way.

3.3.5 Algorithm for Improved Accuracy of Impact Point Prediction

For the proposed impact location prediction algorithm, the forces acting on the projectile are computed using Eqs. 18 to 22. The accelerations of the projectile derived by these forces are integrated twice (using Euler integration) to obtain the velocities and positions using:

$$\boldsymbol{v}(t_{\mathrm{n+1}}) = \dot{\boldsymbol{v}}(t_{\mathrm{n}})\Delta t + \boldsymbol{v}(t_{\mathrm{n}}) \tag{24a}$$

$$\boldsymbol{x}(t_{\mathrm{n+1}}) = \frac{1}{2}\dot{\boldsymbol{v}}(t_{\mathrm{n}})\Delta t^2 + \boldsymbol{v}(t_{\mathrm{n}})\Delta t + \boldsymbol{x}(t_{\mathrm{n}}) \tag{24b}$$

where the constant time interval for the integration is Δt.

The updated positions and velocities are then the initial inputs for the following time interval. After each integration step the aerodynamic coefficients are updated using the nominal data, the standard atmosphere and gravity model. A simplified gravity model has been used for this study using a linear fit of the WGS 84[3] model

$$g = g_0 + g_1 \cdot h \tag{25}$$

where: g_0 = y-intercept ($9.808\,410\,2\ \mathrm{m\,s^{-2}}$)
g_1 = gradient ($-3.070\,952\,3 \times 10^{-6}\ \mathrm{s^{-2}}$)

The above algorithm is repeated until the projectile passes the target altitude (criteria to determine the impact), providing the time to go t_{go} and the lateral and longitudinal impact point for calculating the ZEM offsets by Eq. 13.

4 Simulations and Results

This chapter contains the trajectory simulations which have been performed to compare the performance of three different guidance methods. These are Proportional Navigation (PN) and Zero-Effort-Miss (ZEM), where the later is implemented with two distinct impact prediction methods MPM1 (Sec. 3.2) and MPM2 (Sec. 3.3). First, the guidance is evaluated in the nominal trajectory, thereafter, the guidance is used in Monte-Carlo trajectory simulations applying uncertainties on various initial conditions, aerodynamic coefficients and parameters. All simulations consider perfect navigation and the maximum actuator deflection is set to ±30°.

[3] World Geodetic System (WGS), with the linear fit performed at the cannon position

4.1 Nominal Trajectory

The nominal trajectory of a projectile is defined as a ballistic flight impacting in the target location without uncertainties. The initial conditions are shown in Tab. 2, where the initial spin rate p_0 is obtained by a direct relation of the twist of the barrel and the initial velocity V_0. The target is located 24 km downrange from the cannon for the considered scenario.

Table 2 Initial conditions of nominal trajectory

State	Value	Unit
V_0	940	$\mathrm{m\,s^{-1}}$
p_0	305	Hz
Θ_0	42	°
Ψ_0	0	°

To compare PN (baseline), and the two ZEM guidance techniques the pitch-yaw guidance and control is initiated at 60 s flight time resulting in an approximated time to go t_{go} of less than 21 s. At that flight point, the Line-of-Sight (LoS) rate is small enough to initiate the PN guidance, without exceeding an actuator deflection of ±8° for the nominal trajectory.

The sampling time Δt (Eq. 24) used for the MPM2 IPP (Sec. 3.3) is chosen by evaluating the obtained accuracy in comparison with the necessary computational effort to calculate the estimated impact location. It can be directly (Fig. 5) seen that the sampling time has a much larger impact on the estimation in downrange direction and is therefore considered as critical. The accuracy improves with a higher sampling rate but converges at a sampling time around 100 Hz = 0.01 s. The computational effort increases proportionally to the sample rate. A trade-off between accuracy and computational effort leads to a sampling time of 25 Hz = 0.04 s indicated by the red dotted line. Comparing the two evaluated starting points for the IPP (t = 23 s and 60 s) shows, that the sampling rate of 25 Hz delivers acceptable results independently of the selected starting point for the MPM2 IPP.

Comparing the MPM1 and MPM2 IPP trajectory results (Fig. 6), a large reduction in the predicted offsets, ideally zero, of the nominal trajectory is observed. This reduced ZEM offsets lead directly to much lower commanded accelerations of the ZEM guidance with MPM2 IPP and the autopilot requires smaller actuator deflections. In relation to the baseline PN guidance both ZEM guidance methods have higher control performance reserves by demanding lower actuator deflections. The ZEM guidance with MPM2 IPP is close to the ideal solution of zero actuator demand for the nominal trajectory.

The ZEM commands from MPM2 IPP (Sec. 3.3) are comparable to the accelerations acting on the projectile in the nominal ballistic trajectory (Fig. 6b). The initial perturbations at the beginning are caused mainly by the regulation loop of the pitch-yaw autopilot which has to adapt to the given flight instance displacing the

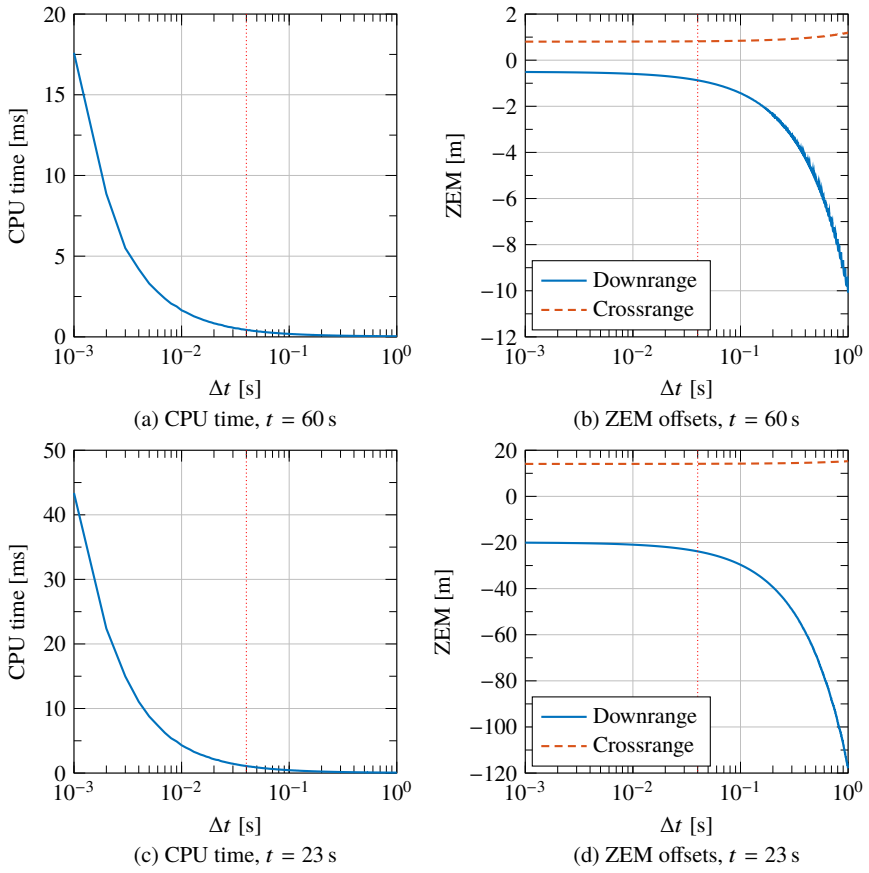

(a) CPU time, $t = 60\,\mathrm{s}$ (b) ZEM offsets, $t = 60\,\mathrm{s}$

(c) CPU time, $t = 23\,\mathrm{s}$ (d) ZEM offsets, $t = 23\,\mathrm{s}$

Fig. 5 Influence of MPM2 IPP sampling time Δt on accuracy and CPU time at $t = 23\,\mathrm{s}$ and $60\,\mathrm{s}$. Vertical dotted red line indicates $25\,\mathrm{Hz} = 0.04\,\mathrm{s}$
Machine: Intel Xeon CPU E5-1607 v2 @3.00 GHz with 4 physical cores and 16 GB RAM

impact position and forcing the ZEM guidance to command an acceleration in the opposite direction. Towards the end of the trajectory, the ZEM guidance suffers from the time to go singularity, which is caused by the nominator of the navigation gain k_g (Eq. 16). Therefore, a different guidance method e.g. modified PN should be used for the end game task. For this study, the endgame is performed by PN guidance if the distance to the target is less than 50 m.

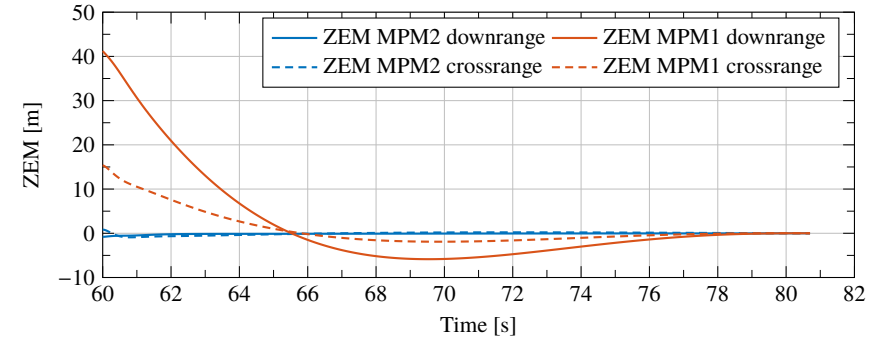

(a) ZEM offsets

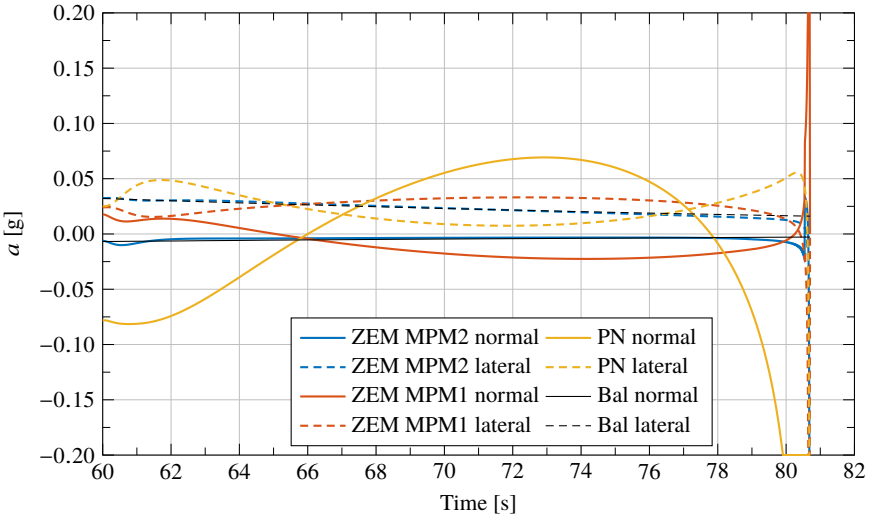

(b) ZEM and PN acceleration command and ballistic acceleration

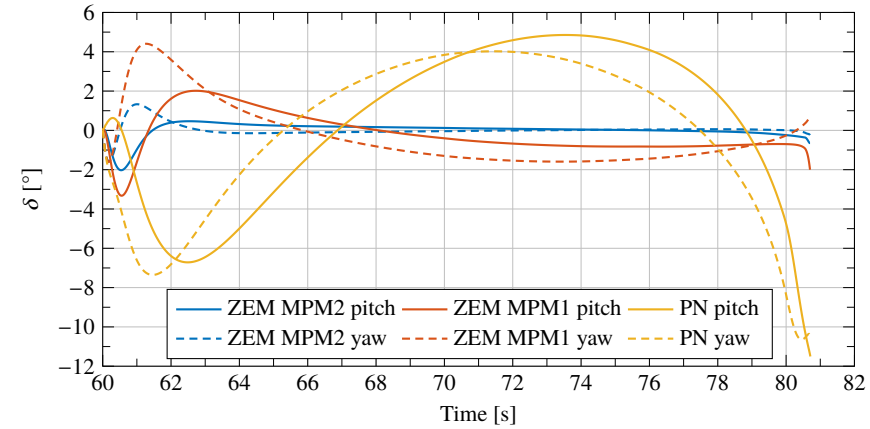

(c) Actuator deflection angle

Fig. 6 Comparing IPP algorithm performance of Sec. 3.2 and 3.3

4.2 Monte-Carlo Trajectories

Monte-Carlo methods are used for trajectory simulations to study the influence of certain parameters by using repeated random sampling to obtain the numerical results. Here, it is used to evaluate the influence of uncertainties (Tab. 3) on the initial states (velocity V_0, elevation Θ_0, azimuth Ψ_0), the aerodynamic coefficients (axial force C_X, normal force slope $C_{N\alpha}$) and the environmental parameters (pressure P, temperature T, longitudinal wind u_w, lateral wind v_w). To obtain a sample of trajectories which is large enough to provide representative results, 2000 individual cases are simulated; each one using a set of normally distributed random uncertainties. The nominal trajectory (Sec. 4.1) is considered as the reference for these simulations.

Table 3 Uncertainties used for Monte-Carlo Trajectories

Parameter	σ	Unit
V_0	5	$\mathrm{m\,s^{-1}}$
Θ_0	1.5	$^\circ$
Ψ_0	2.5	$^\circ$
C_X	1	%
$C_{N\alpha}$	3	%
P	0.4	%
T	0.4	%
u_w	3.5	$\mathrm{m\,s^{-1}}$
v_w	3.5	$\mathrm{m\,s^{-1}}$

The simulation results obtained concern the relative impact distributions (Fig. 7), the miss distances (Fig. 8a) and finally the maximum necessary actuator deflections (Fig. 8b). The above results are compared for three guidance strategies: the first is PN-based whereas the second and third ones are ZEM MPM2 IPP-based. The difference between the last two ones is only the guidance starting time ($t = 60\,\mathrm{s}$ and $t = 23\,\mathrm{s}$ respectively). In fact, given that the ZEM MPM2 IPP-based method permits an earlier start of the guidance (contrary to the PN-based) since no approximately LoS constraint is required, there is a clear benefit from this strategy. For completeness, the ballistic trajectories are also illustrated together with the guided ones.

Referring to Fig. 7, the total ballistic dispersion (top left) that needs to be corrected from the guidance was found to be up to $\pm 500\,\mathrm{m}$ in crossrange and $\pm 1000\,\mathrm{m\,m}$ in downrange based on the considered uncertainties of Tab. 3. The PN-based method reduces the dispersion to 2.264 m of CEP[4] and the ZEM MPM2 IPP-based to almost zero. However, it must be noted that in the latter strategy, there is a big improvement concerning the $1\,\sigma$, $2\,\sigma$ and $3\,\sigma$. Referring to Fig. 8, the maximum miss distance and actuator deflection are also greatly reduced.

[4] For information, the Circular Error Probable (CEP) is here defined as the maximum miss distance of the first 50 % of all trajectories when ordered from low to high miss distances. Same definition applies for $1\,\sigma = 68.2\,\%$, $2\,\sigma = 95.4\,\%$ and $3\,\sigma = 99.7\,\%$.

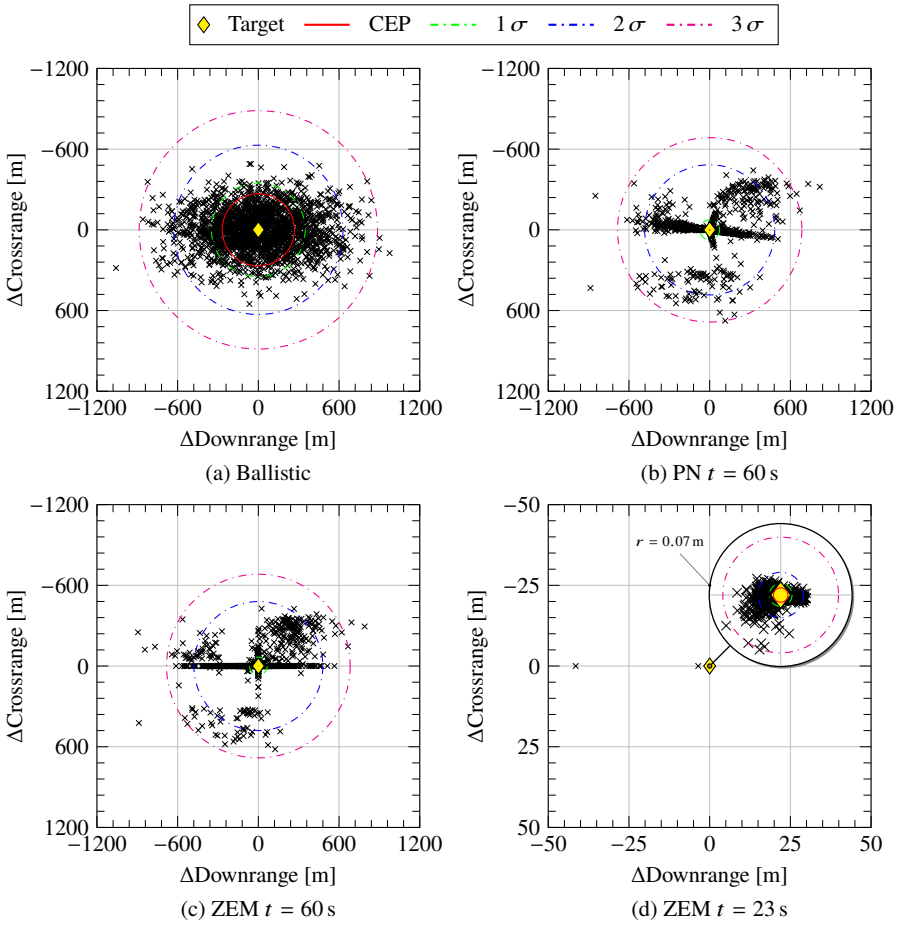

Fig. 7 Relative impact distributions at a range of 24 km. ZEM uses MPM2 IPP

Table 4 Impact distributions

Guidance Method	CEP [m]	1 σ [m]	2 σ [m]	3 σ [m]
Ballistic	268.620	348.572	629.209	886.122
PN (t = 60 s)	2.264	73.769	483.610	685.482
ZEM MPM2 IPP (t = 60 s)	0.077	66.055	479.505	682.494
ZEM MPM2 IPP (t = 23 s)	0.007	0.011	0.022	0.056

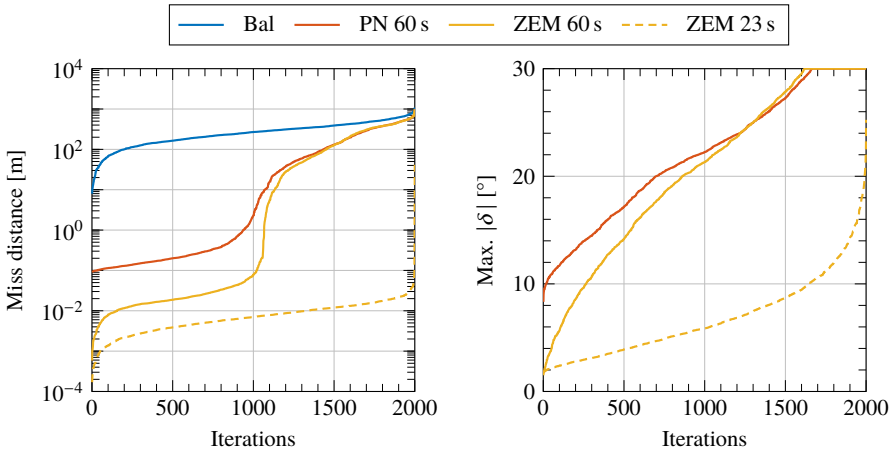

(a) Miss distance

(b) Maximum actuator deflection

Fig. 8 Miss distance and maximum actuator deflection angle distributions. ZEM uses MPM2 IPP

5 Conclusions and Future Work

This paper presents an Impact Point Prediction (IPP) method for a 155 mm, canard-guided, spin-stablized projectile. This IPP method is used for a Zero-Effort-Miss (ZEM) guidance to improve the ballistic impact distribution to minimize the miss distance to the target and several existing categories of IPP methods are discussed. One existing Modified Point Mass (MPM1) model is analyzed to improve the accuracy, and from that knowledge a second MPM2 model is developed alleviating the shortcomings of the previous method. Concerning the nominal trajectory, the latter model is compared against Proportional Navigation (PN) guidance and a ZEM guidance (using the MPM1 model). The results show a considerable reduction in the prediction error, and a noticeable decrease of the guidance acceleration command and required actuator control deflection. Concerning the non-nominal trajectories, Monte-Carlo simulations with uncertainties in the launch condition, aerodynamic coefficients and environmental parameters are performed, demonstrating an important improvement on the guidance performance of ZEM with MPM2 IPP.

Future work will focus on the robustness of the IPP when using imperfect navigation data, additional uncertainties (e.g. more aerodynamic coefficients or projectile constants) and the induced jump in the ZEM guidance command due to the sign change resulting from high elevation angles.

References

1. Burchett, B., Peterson, A., Costello, M.: Prediction of swerving motion of a dual-spin projectile with lateral pulse jets in atmospheric flight. Mathematical and Computer Modelling **35**, 821–834 (2002)
2. Corriveau, D., Wey, P., Berner, C.: Thrusters pairing guidelines for trajectory corrections of projectiles. Journal of Guidance, Control, and Dynamics **34**(4), 1120–1128 (2011)
3. Costello, M., Peterson, A.: Linear theory of a dual-spin projectile in atmospheric flight. Journal of Guidance, Control, and Dynamics **23**(5), 789–797 (2000)
4. Fresconi, F.: Guidance and control of a projectile with reduced sensor and actuator requirements. Journal of Guidance, Control, and Dynamics **34**(6), 1757–1766 (2011)
5. Fresconi, F., Cooper, G., Costello, M.: Practical assessment of real-time impact point estimators for smart weapons. Journal of Aerospace Engineering **24**, 1–11 (2011)
6. Gagnon, E., Vachon, A.: Efficiency analysis of canards-based course correction fuze for a 155-mm spin-stabilized projectile. Journal of Aerospace Engineering pp. 1–10 (2016)
7. Hahn, P.V., Frederick, R.A., Slegers, N.: Predictive guidance of a projectile for hit-to-kill interception. IEEE Transactions on Control Systems Technology **17**(4), 745–755 (2009)
8. Lieske, R.F., Reiter, M.L.: Equations of motion for a modified point mass trajectory. Tech. rep., Ballistic Research Laboratory (1966)
9. Ollerenshaw, D., Costello, M.: Simplified projectile swerve solution for general control inputs. Journal of Guidance, Control, and Dynamics **31**(5), 1259–1265 (2008)
10. Rogers, J., Costello, M.: Control authority of a projectile equipped with a controllable internal translating mass. Journal of Guidance, Control, and Dynamics **31**(5), 1323–1333 (2008)
11. Theodoulis, S., Gassmann, V., Wernert, P., Dritsas, L., Kitsios, I., Tzes, A.: Guidance and control design for a class of spin-stabilized fin-controlled projectiles. Journal of Guidance, Control, and Dynamics **36**(2), 517–531 (2013)
12. Theodoulis, S., Sève, F., Wernert, P.: Robust gain-scheduled autopilot design for spin-stabilized projectiles with a course-correction fuze. Aerospace Science and Technology **42**, 477–489 (2015)
13. Wernert, P.: Simulations de trajectoires de projectiles à 6 degrés de liberté dans le cadre de la mécanique du vol avion. partie 3 : Utilisation de repéres non liés au projectile. Tech. rep., ISL (2007)
14. Zarchan, P.: Tactical and Strategic Missile Guidance, 6th edn. Progress in Astronautics and Aeronautics. American Institute of Aeronautics and Astronautics, Reston, VA, USA (2012). DOI 10.2514/4.868948
15. Zipfel, P.H.: Modeling and Simulation of Aerospace Vehicle Dynamics. AIAA Education Series (2007)